Mon. Not. R. Astron. Soc. **344,** 1107–1118 (2003)

The identification of HCN and HNC in carbon stars: model atmospheres, synthetic spectra and fits to observations in the 2.7–4.0 μm region

G. J. Harris,[1⋆] Ya. V. Pavlenko,[2] H. R. A. Jones[3] and J. Tennyson[1]

[1]*Department of Physics and Astronomy, University College London, London WC1E 6BT*
[2]*Main Astronomical Observatory, National Academy of Sciences, Zabolotnoho 27, Kyiv-127 03680, Ukraine*
[3]*Astrophysics Research Institute, Liverpool John Moores University, Twelve Quays House, Egerton Wharf, Birkenhead CH41 1LD*

Accepted 2003 June 4. Received 2003 June 2; in original form 2003 April 11

ABSTRACT

Model carbon star atmospheres and synthetic spectra have been calculated using the recent HCN/HNC vibration rotation line list of Harris et al. The calculations are repeated using only HCN lines and show that HNC has a significant effect upon the temperature, density and optical depth of a stellar atmosphere.

We fit synthetic spectra in the 2.7–4.0 μm region to observed *ISO* spectra of the carbon stars WZ Cas and TX Psc obtained by Aoki et al. These fits allow us to identify absorption by HNC in the spectrum of WZ Cas at 2.8–2.9 μm, and to determine new independent estimates of effective temperature and log $(N_{\rm C}/N_{\rm O})$. The findings reported here indicate that absorption by both HCN *and* HNC is needed to fully explain the observed stellar spectra and represent the first identification of HNC in a star. Q-branch absorption by the HCN $\Delta v_2 = 1$, $\Delta v_3 = 1$ and $\Delta v_1 = 1$, $\Delta v_2 = -1$ bands at 3.55 and 3.86 μm, respectively, is identified in the spectrum of WZ Cas.

Key words: molecular data – stars: AGB and post-AGB – stars: atmospheres – stars: carbon – infrared: stars.

1 INTRODUCTION

It is well known that HCN is an important opacity source in carbon stars and one that can dramatically affect the structure of the atmospheres of these stars (Eriksson et al. 1984; Jørgensen et al. 1985). It is therefore vital that the opacity of this particular molecule should be accurately accounted for. Several recent works have used different sources of HCN opacity data. The recent carbon-rich model atmosphere calculations of Aoki, Tsuji & Ohnaka (1998, 1999) used the HCN band transition dipoles and molecular constants determined experimentally by Maki, Quapp & Klee (1995) and Maki et al. (1996) to account for HCN opacity. In contrast, other recent works (Loidl et al. 1999; Loidl, Lançon & Jørgensen 2001; Jørgensen, Hron & Loidl 2000) have used the *ab initio* data of Jørgensen et al. (1985). Although *ab initio* data cannot rival laboratory data in accuracy, laboratory data are limited to a tiny fraction of the billions of possible HCN transitions. As a consequence, the laboratory data cannot possibly account for all of the HCN opacity. This makes *ab initio* data more useful for high-temperature calculations, which require a more complete description of molecular vibration–rotation spectra and hence opacity. The *ab initio* data of Jørgensen et al. (1985) were the first extensive HCN opacity data set, and were a step forward from the empirical estimates of HCN opacity used by Eriksson et al. (1984). However, over the intervening decade and a half, the advances in molecular quantum-mechanical techniques coupled with increasingly more powerful computers have improved the quality and quantity of spectroscopic calculations on triatomic molecules. These improvements enabled the calculation of the extensive HCN and HNC line list of Harris, Polyansky & Tennyson (2002b), which we use in this work. The line list of Harris et al. (2002b) is both more extensive and more accurate than the data of Jørgensen et al. (1985).

A further advantage of the line list of Harris et al. (2002b) over those of Jørgensen et al. (1985) and Aoki et al. (1998) is that it also takes into account the effect of the HNC isomer of HCN. Recent calculations by Barber, Harris & Tennyson (2002) have yielded an HNC to HCN ratio, at thermodynamic equilibrium, of 0.13 at 2600 K and 0.19 at 3000 K. This, coupled with the fact that the band transition dipoles of the fundamental bands of HNC are stronger than their HCN counterparts, implies that HNC will contribute to the opacity of C-star atmospheres.

To determine the effect that the new opacity data of Harris et al. (2002b) have on model C-star atmospheres and synthetic spectra, we present a grid of model atmospheres calculated using these data. We then discuss these model atmospheres and compare them with existing C-star model atmospheres. We compare the synthetic spectra with existing *ISO* observations of the C stars TX Psc and WZ Cas

⋆E-mail: greg@theory.phys.ucl.ac.uk

in the 2.7–4.0 μm region. This spectral region lies between the two strong CO bands, $\Delta v = 1$ and 2, and contains several discernible HCN bands and the HNC H–N stretch fundamental band. From this comparison we determine effective temperatures and C/O ratios for these stars. The effect of HNC opacity is identified for the first time in the spectrum of WZ Cas, and we attempt to identify Q branches of two HCN modes in the spectra of WZ Cas.

2 HCN AND HNC

The HCN/HNC line list of Harris et al. (2002b) covers transitions between all HCN and HNC energy levels below 18 000 cm^{-1} above the HCN zero-point energy and with angular momentum quantum number $J \leqslant 60$. There are approaching 400 million lines and around 125 000 vibration–rotation energy levels in this line list. The accuracy of the results of this calculation in room-temperature situations has been discussed in Harris, Polyansky & Tennyson (2002a). In particular, it was found that the band transition dipoles calculated from this line list were within combined systematic and experimental errors. All the fundamental band centres are displaced from the laboratory values by less than 4 cm^{-1}, except for the HNC H–N stretch fundamental, which has an error of 12.5 cm^{-1}. The rotational error, corrected for vibrational error, for the lines of the fundamental vibrational modes of HCN/HNC are less than 0.7 cm^{-1} at $J = 20$ (van Mourik et al. 2001). Many of the lines in the line list are extremely weak and make no real contribution to the overall opacity. We therefore reduce the number of lines used in the calculation of the model atmospheres and synthetic spectra by cutting out lines based on absolute intensity. We used a minimum absolute intensity at 3000 K of 10^{-15} cm^{-2} atm^{-1}; the strongest lines are of the order of 0.1 cm^{-2} atm^{-1}. This truncation dramatically reduced the number of lines, with little effect on the overall opacity. For the model atmospheres, lines were also selected on the basis of proximity to one of the frequency points used in the calculation. We must correct an error in the value of the constant given in equation (1) of Harris et al. (2002b). This constant should read $3.565\,89 \times 10^{7}$, and not $3.507\,29 \times 10^{-6}$.

To show clearly the effect of HNC opacity on the atmospheres of C stars, it is necessary to separate the combined HCN/HNC line list of Harris et al. (2002b) into HCN and HNC data. As there are 125 000 energy levels in the line list of Harris et al. (2002b), it would be very time-consuming and tedious to identify by hand energy levels as HCN or HNC. Consequently we used the identification algorithm used by Harris et al. (2002a). In this method individual energy levels are labelled HCN or HNC on the basis of the strengths of the transition from that level to the vibrational ground HCN and HNC states. An energy level that has a transition dipole to the ground state of HCN that is several orders of magnitude stronger than the transition to the ground HNC state can confidently be identified as HCN and vice versa. Two problems arise with this method. The first and most important involves energy levels that have very weak transitions to the ground state. For example the HCN (0, 8, 8, 0) → (0, 0, 0, 0) band is forbidden by the normal dipole transition rules for a linear triatomic ($\Delta l = -1, 0, +1$). This transition is so weak that it is below the noise level in the calculation, and states with a transition to the ground state this weak we do not assign as HCN or HNC. Secondly, the idea that HCN and HNC are separate molecules is incorrect at high energies. The wavefunctions of some high-lying states have magnitude in both HCN and HNC potential wells and so cannot be described as HCN or HNC – these are called 'delocalized' states. Such states can have transitions to the HCN and HNC ground states that are of roughly the same order of magnitude.

The calculations that we make in this work which are described as 'HCN only' exclude only the HNC levels that we can confidently identify. There may be other HNC energy levels in the data that are unassigned. However, these 'HCN only' data will exclude the strongest HNC transitions and will allow us to identify the effect of HNC on our model atmospheres and spectra. We label energy levels confidently identified as HCN as $i = 0$, HNC levels as $i = 1$, delocalized states as $i = 2$ and unassigned states as $i = 3$. Fig. 1 shows

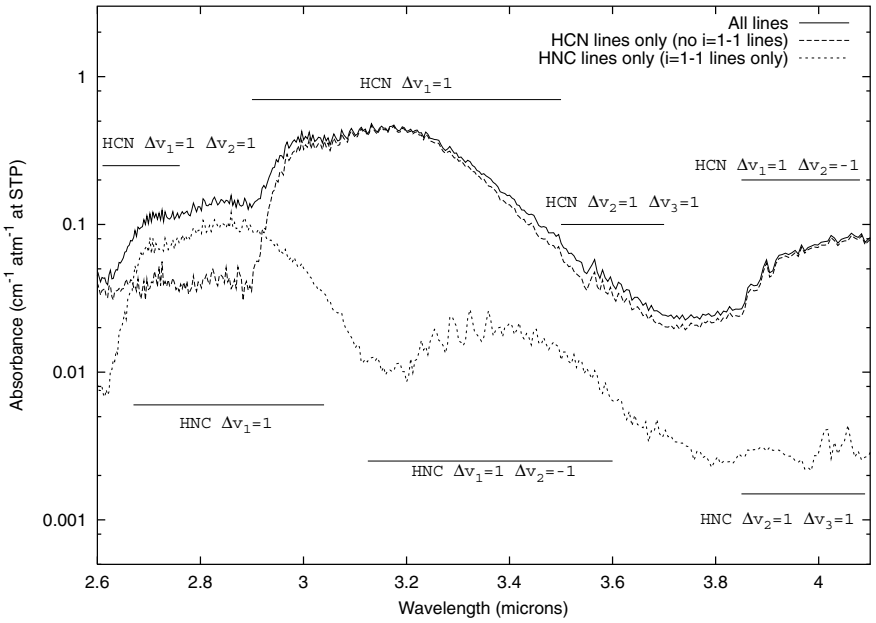

Figure 1. The wavelength-dependent absorbance of HCN and HNC. The three curves represent the absorbance of HCN/HNC (all lines), the absorbance of HCN only (all lines except $i' = 1, i'' = 1$) and the absorbance of HNC (lines with $i' = 1, i'' = 1$). The main HCN and HNC features are labelled. See text for a full description of *i*.

a plot of HCN and HNC absorbance at $T = 3000$ K as a function of wavelength, from 2.6 to 4.1 μm. The three curves show absorbance calculated with all lines, absorbance calculated with HCN lines only, and absorbance calculated only with confidently identified HNC lines. Over this spectral range HNC absorption only exceeds that of HCN at wavelengths between 2.7 and 2.9 μm. However, between 3.2 and 3.9 μm HNC appears to contribute significantly (10–15 per cent) to the total opacity. The effect of this HNC absorption can be seen in our synthetic spectra (see Sections 5.2.1 and 5.2.2).

We have used the recent *ab initio* HCN/HNC partition function of Barber et al. (2002) in all of our calculations. This partition function was calculated by direct summation using the HCN/HNC energy levels of Harris et al. (2002b) up to $J = 32$ and includes an extrapolation of these levels up to $J = 91$, which is enough to rotationally converge the partition function. The error of this partition function has been estimated to be 0.6 per cent at $T = 2600$ K and of 0.8 per cent at $T = 3000$ K (Barber et al. 2002); HNC energy levels are also included in the calculation.

3 STELLAR SPECTRA

The spectral region required for this programme is difficult to obtain from ground-based observatories and is well matched to *ISO* capabilities. In particular the SWS instrument on *ISO* provides sufficient resolution to resolve individual vibration–rotation bands. The observations used for this study were taken as part of the Japanese guaranteed observing time (REDSTAR1, PI T. Tsuji, e.g. Aoki et al. 1998). This programme obtained a number of infrared measurements of carbon stars. For the purposes of our study we selected the high-resolution observations made for TX Psc (N-type) and WZ Cas (SC-type) from the *ISO* archive facility.

The observations were made with the Short Wavelength Spectrometer (SWS) in its full resolution grating mode known as SWS06. Here we use spectra with a resolution of 1000–2000 from bands 1B, 1D and 1E covering the wavelength ranges 2.74–3.02, 3.02–3.52 and 3.52–4.08 μm. The observational data are scientifically validated and were processed using the standard archive reduction software. The spectra were inspected using the *ISO* Spectral Analysis Package to check for glitches and bad data points. Aoki et al. (1998) note that the flux discrepancies are at most 10 per cent for the REDSTAR1 data set. For the subset of data used for this paper, we find that the flux calibration errors between SWS bands are at the level of a few per cent, as expected for band 1 SWS observations. The wavelength calibration for the SWS instrument is measured to be within one-eighth of a resolution element Salama et al. (1997).

4 PROCEDURE

4.1 Ionization–dissociation equilibrium

In atmospheres of cool ($T_{\rm eff} < 6500$ K) carbon-rich stars, the ionization–dissociation equilibrium is governed by the CO molecule, that is, the densities of carbon-containing species depend on the C/O ratio (see Tsuji 1973 for more details). The ionization–dissociation equilibrium is computed for ∼100 species including the most abundant carbon-containing molecules. Constants of chemical equilibrium for most species are taken from Tsuji (1973) and constants for HCN are converted into our model atmosphere format using partition function data of Barber et al. (2002) following the scheme of Pavlenko (2002b). HCN and HNC molecules are treated as a single molecule with a single partition function and dissociation potential.

4.2 Opacities

The standard set of continuum opacities included in ATLAS12 by Kurucz (1996) are used. Computations of a few opacities were added or upgraded: the absorption of C^- (Myerscough & McDowell 1966) and H_2^- (Doyle 1968).

To compute the opacities due to bound–free absorption of C, N and O atoms, we used TOPBASE (Seaton, Zeipen & Tully 1992). Cross-sections are available on http://www.mao.kiev.ua/staff/yp/. See Pavlenko & Zhukovska (2003) for more details.

To compute the opacities due to bound–bound absorption of atoms and molecules in atmospheres of C giants, we used line lists from different sources

(i) Electronic and vibration–rotation line data of diatomic molecules (CN, C_2, MgH, H_2, SiH, CO) were taken from CD-ROM 18 of Kurucz (1993). For synthetic spectra computations, we used the vibration–rotation lines of CO from Goorvitch (1994).

(ii) Atomic line data were taken from VALD (Kupka et al. 1999).

(iii) HCN/HNC vibration–rotation lines were taken from Harris et al. (2002b); see Section 2.

(iv) CS vibration–rotation lines were taken from Chandra et al. (1995).

Other works (Aoki et al. 1998, 1999; Jørgensen et al. 2000) have included C_2H_2 opacity. For warmer C stars, such as WZ Cas and TX Psc, C_2H_2 has only a small effect on opacity (Aoki et al. 1998). Hence it is not necessary to include H_2C_2 within our calculations. However, for cooler C stars with high $\log(N_{\rm C}/N_{\rm O})$, H_2C_2 may well be more important and should be included within the calculation.

For the model atmosphere calculations, we used the opacity sampling approach Sneden, Johnson & Krupp (1976) to account for the absorption by atomic and molecular lines. Absorption of the molecular electronic bands

CaO ($C^1\Sigma - X^1\Sigma$),	NO ($C_2\Pi_r - X_2\Pi_r$),
CS ($A^1\Sigma - X^1\Sigma$),	NO ($B_2\Pi_r - X_2\Pi_r$),
SO ($A^3\Pi - X^3\Sigma$),	NO ($A^2\Sigma^+ - X_2\Pi_r$),
SiO ($E^1\Sigma - X^1\Sigma$),	MgO ($B^1\Sigma^+ - X^1\Sigma^+$),
SiO ($A^1\Pi - X^1\Sigma^+$,	AlO ($C^2\Pi - X^2\Sigma$),
	AlO ($B^2\Sigma^+ - X^2\Sigma^+$),

are taken into account by the just overlapping line approach (JOLA), using the subprograms of Nersisian, Shavrina & Yakemchuk (1989). In general, these molecules absorb in the blue part of the spectrum and their bands are not principal opacity sources in stellar atmospheres. Nevertheless, the JOLA algorithm enables us to reproduce both the relative strength and shapes of the spectral energy distributions for late-type stars (Pavlenko 1997, 2000).

4.3 Model atmospheres

We computed a grid of model atmospheres of C giants with the SAM12 program Pavlenko (2002a, 2003), which is a modification of ATLAS12 (Kurucz 1996). SAM12 is a classical model atmospheres code: plane-parallel media, local thermodynamic equilibrium (LTE), no sources and sinks of energy within the atmosphere, energy transferred by radiative field and convection. Convection is treated in the frame of mixing length theory (in our computations we adopt $l/H = 2.0$) and convective overshooting (Kurucz 1996) was not considered. Opacity sampling treatment (Sneden at al. 1976) is used to account for atomic and molecular absorption. We investigate the sensitivity of our synthetic spectra to changes in effective temperatures $T_{\rm eff}$, abundances of carbon $\log N$(C) and microturbulent velocities $V_{\rm t}$. We adopt the 'solar values' of Anders & Grevesse

(1989) for elements other than carbon; for example, oxygen log $N(\mathrm{O}) = -3.12$ is adopted where $\sum N_i = 1$.

Model atmospheres were computed for effective temperatures of $T_{\rm eff} = 2500$–3500 K, carbon abundances of log $N(\mathrm{C}) = -3.19$ to -3.09, and carbon isotopic ratios of $^{12}\mathrm{C}/^{13}\mathrm{C} = 3$–$10$. Around 100 model atmospheres were generated for this work. The models computed with the complete HCN/HNC line list are available from http://www.mao.kiev.ua/staff/yp/Results, as files Mod.Cg10.tar.gz and Mod.Cg03.tar.gz.

4.4 Synthetic spectra

Numerical computations of theoretical radiative fluxes F_ν were carried out within the same classical approach as our model atmospheres using the WITA6 program (Pavlenko 2000). The shape of every line was determined using the Voigt function $H(a, v)$. We account for natural broadening as well as van der Waals and Stark broadening of lines. Owing to the low temperature and densities of C-giant model atmospheres, Stark broadening may be ignored. Radiative broadening may play a major role in the outermost layers; in deep photospheric layers van der Waals broadening becomes important. Damping constants were taken from line data bases such as VALD (Kupka et al. 1999) or computed following Unsold (1955). The generation of our synthetic spectra is performed using the same opacity source lists and sets of abundances as our model atmospheres. This approach allows us to see directly the impact of abundance changes on the temperature structure of the model atmosphere as well as the synthetic spectra. Computations of synthetic spectra were carried out with wavelength steps of 0.05 nm.

4.5 Fit to observed spectra

There are several parameters that can be adjusted to fit synthetic spectra to observed stellar spectra. The most important of these include the logarithm of the carbon-to-oxygen ratio log $(N_{\rm C}/N_{\rm O})$, effective temperature $T_{\rm eff}$, surface gravity log g, metallicity log $(Z/Z_\odot)$, and turbulent velocity $V_{\rm t}$. Fits obtained by varying these parameters are often not unique; for example, Jørgensen et al. (2000) obtained two good fits for TX Psc, with different values of these parameters. In this work we attempt to gain good fits to the observed stellar spectra with log $(N_{\rm C}/N_{\rm O})$ and $T_{\rm eff}$, but if necessary we change $V_{\rm t}$ and the metallicity.

To obtain a fit we fix log g to 0.0; this value was estimated by Aoki et al. (1998) from a measured radius of 200 $\mathrm{R}_\odot$ for TX Psc and an assumed mass of between 1 and 2 $\mathrm{M}_\odot$. We also fix $V_{\rm t}$ to 3.5 km s^{-1} and metallicity to solar values, then calculate synthetic spectra on a log $(N_{\rm C}/N_{\rm O})$, $T_{\rm eff}$ grid. When a reasonable fit is found, we adjust log $(N_{\rm C}/N_{\rm O})$ and $T_{\rm eff}$ to obtain a better fit, and if necessary change $V_{\rm t}$ and metallicity to improve the fit further. We did not find it necessary to change log g to obtain good fits. Normalization of the synthetic spectra and stellar spectra was carried out by dividing through by the Planck function of the relevant $T_{\rm eff}$, then scaling the spectra so that the maximum flux is unity. The temperature of the blackbody spectrum used to normalize the stellar spectra is the $T_{\rm eff}$ of the best-fitting synthetic spectrum. The division of the observed spectra by the Planck function is adequate to normalize the spectrum to a pseudo-continuum.

5 RESULTS

The calculations reported here are the first to use the new HCN/HNC data of Harris et al. (2002b). The fact that the data of Harris et al. (2002b) contains more lines implies a greater atmospheric opacity than accounted for in preceding HCN/HNC data (Jørgensen et al. 1985; Aoki et al. 1998). This increased opacity may have a significant effect on both the structure and spectra of our model atmospheres and synthetic spectra.

5.1 Model atmospheres

Fig. 2 shows a plot of pressure versus temperature for nine different model atmospheres with a log $(N_{\rm C}/N_{\rm O})$ of 0.01, temperatures of

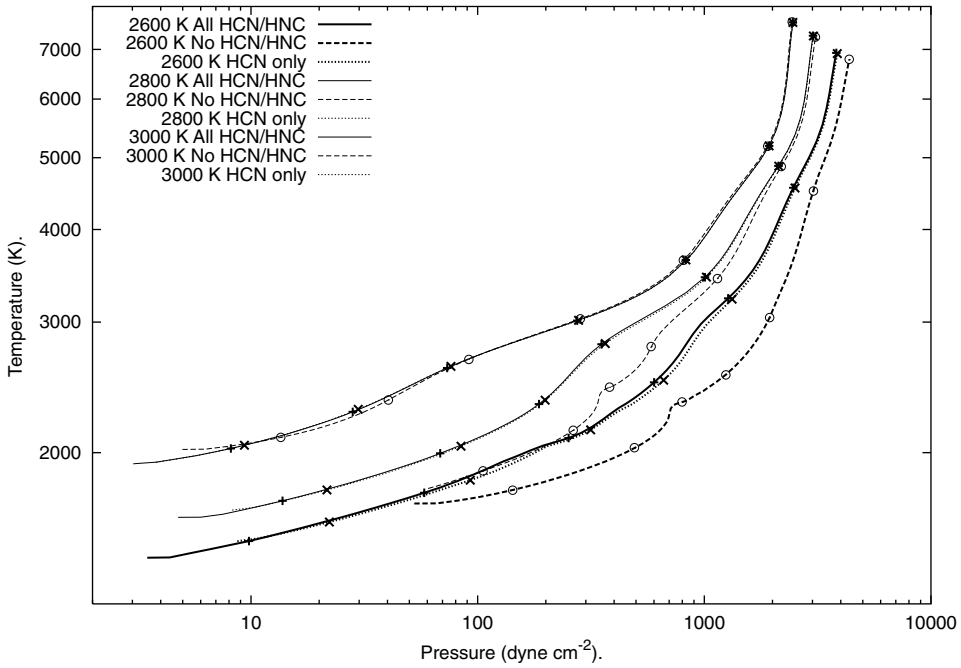

Figure 2. Plot of pressure versus temperature on logarithmic scales for models with HCN/HNC lines (solid lines, + symbols), with HCN lines only (dotted lines, × symbols) and without any HCN/HNC lines (dashed lines, ° symbols), at $T = 2600$ K (thick), 2800 K (medium) and 3000 K (thin), with log $(N_{\rm C}/N_{\rm O})$ of 0.01. Symbols are placed at Rosseland optical depths of log $\tau_{\rm R} = -4, -3, -2, -1, 0, 1, 2, 3$.

2600, 2800 and 3000 K, and with HCN/HNC opacity, with only HCN opacity and without HCN/HNC opacity. Symbols are placed on the curves at values of log τ_R of −4, −3, −2, −1, 0, 1 and 2. The difference between the model atmospheres with and without HCN/HNC opacity at 2800 and 2600 K is considerable. At a given optical depth the atmospheres with HCN/HNC opacity are cooler and at a much lower pressure, which is consistent with the trends originally reported by Eriksson et al. (1984). However, in the model atmospheres with an effective temperature of 3000 K, most of the HCN/HNC has been destroyed and the differences between spectra with and without HCN/HNC opacity is much reduced. None the less these differences are still significant, especially in the outer parts of the atmosphere. The model atmospheres with HCN/HNC and with only HCN have discernible differences. At a given optical depth the models with HCN opacity only are hotter and at higher pressures than the models with HCN/HNC opacity. Much of this change in the optical depth pressure–temperature relationship is due to the increase in opacity and hence optical depth as a result of HNC absorption. However, some of the differences are also attributable to changes in the pressure–temperature curve of the atmospheres brought about by increased absorption. The change in the pressure–temperature curve is most pronounced in the 2600 K models.

Fig. 3 shows a plot of pressure versus temperature for nine model atmospheres with log (N_C/N_O) of 0.003, 0.01 and 0.03 at a temperature of 2800 K, with and without HCN/HNC opacity and with HCN opacity only. As in Fig. 2 the model atmospheres with HCN/HNC opacity are cooler and at much lower pressure than those without HCN/HNC opacity. It is also clear that the atmospheres with a higher C/O ratio have a hotter, lower pressure atmosphere, which is consistent with the findings of Aoki et al. (1998). The reason is that more carbon-rich molecules can form at higher C/O ratio, resulting in a more opaque, so hotter and less dense, atmosphere. All these pressure–temperature curves are consistent with the model atmospheres reported by Aoki et al. (1998) and Jørgensen et al. (2000). Again there are differences between the models that account for HCN/HNC opacity and the models that account for only HCN opacity.

5.2 Spectra

Fig. 4 shows synthetic spectra calculated at effective temperatures of 2600, 2800, 3000 and 3100 K. At T_{eff} of 2600 and 2800 K the atmospheric temperatures and densities are conducive to the formation of HCN/HNC, so the spectra between 2.7 and 4.0 μm are dominated by HCN absorption. Between 2.9 and 3.4 μm is the characteristic strong absorption feature that is predominantly caused by the H–C stretching mode of HCN. There are strong, narrow absorption features around 3.6 μm caused by HCN Q branches (see below). Immediately either side of the 3.6-μm feature are broader, weaker absorption features corresponding to P and R branches of the same bands. There are also strong, narrow absorption features longwards of 3.8 μm, caused by a combination of CS and HNC bands (see below). Finally the broad absorption around 2.8 μm is caused by the H–N stretching fundamental of HNC and its hot bands. At $T_{eff} = 3000$ K, all these absorption features are weaker; the narrow features at 3.6 μm and longwards of 3.8 μm have all but vanished. The 3.0–3.4 μm feature has narrowed and weakened. The HNC absorption at 2.8 μm is considerably weaker, and the spectrum in this region is becoming dominated by CO. At $T_{eff} =$ 3200 K, almost no trace of HCN and HNC absorption is left, even at 3 μm. Longwards of 2.9 μm the spectrum is flat. These changes are a direct result of the temperature dependence of the HCN and HNC abundance. As the effective temperature increases to 3000 K, the HCN/HNC molecules begin dissociating to form CN; this process is complete by 3200 K, at which point little sign of HCN is present.

Fig. 5 shows synthetic spectra calculated with an effective temperature of 3000 K and with log (N_C/N_O) of 0.03, 0.02, 0.01, 0.003

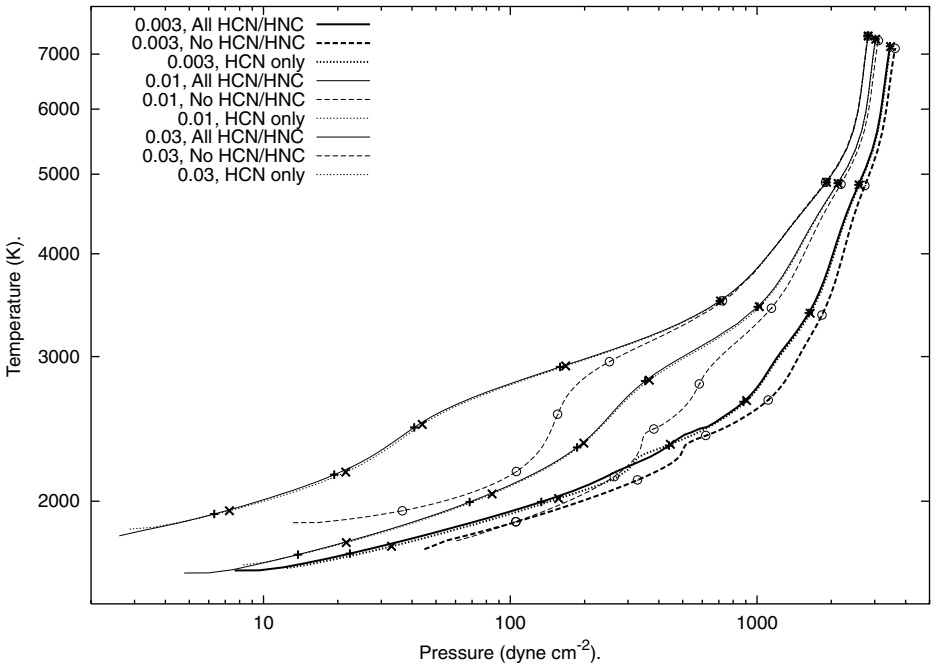

Figure 3. Plot of pressure versus temperature on logarithmic scales for models with HCN/HNC lines (solid lines, + symbols), with HCN lines only (dotted lines, × symbols) and without any HCN/HNC lines (dashed lines, ° symbols), at $T = 2800$ K, with log (N_C/N_O) of 0.003 (thick), 0.01 (medium) and 0.03 (thin). Symbols are placed at Rosseland optical depths of log $\tau_R = -4, -3, -2, -1, 0, 1, 2, 3$.

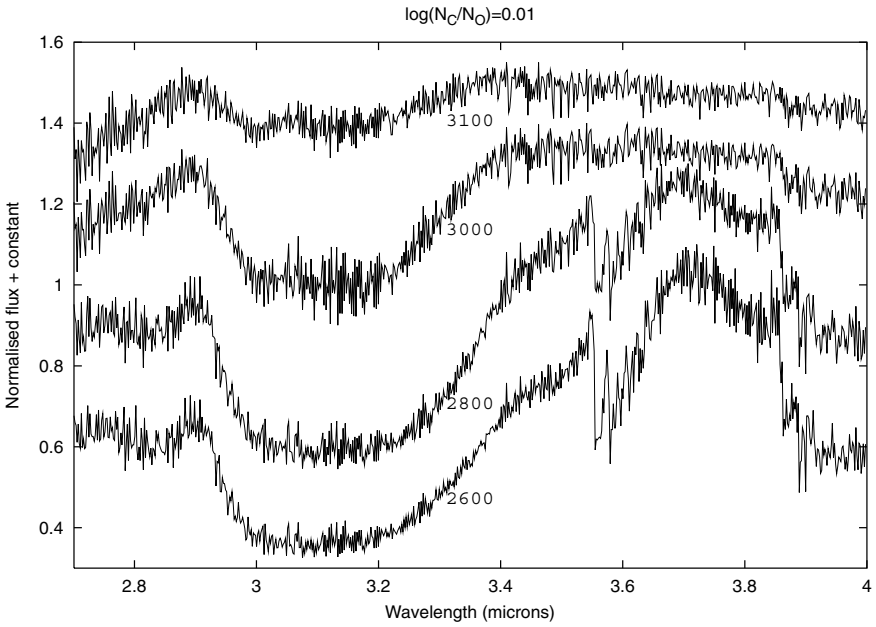

Figure 4. Synthetic spectra with a log (N_C/N_O) of 0.01 and effective temperatures of 2600, 2800, 3000 and 3100 K.

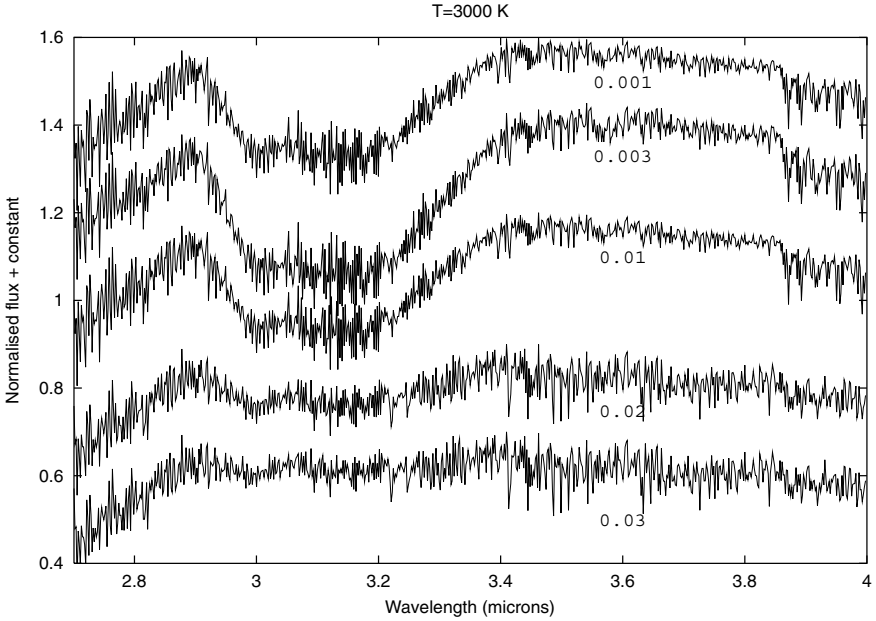

Figure 5. Synthetic spectra with an effective temperature of 3000 K and log (N_C/N_O) of 0.03, 0.02, 0.01, 0.003 and 0.001. A constant has been added to the flux of some of the spectra, to stagger them.

and 0.001. At $T_{\rm eff} = 3000$ K the HCN/HNC abundance is highly sensitive to both the C/O ratio and temperature. This is seen in both Figs 4 and 5. The 3.0–3.4 μm feature is strong for log (N_C/N_O) between 0.001 and 0.01, but is weak at log $(N_C/N_O) = 0.02$ and almost non-existent at log $(N_C/N_O) = 0.03$. Here higher C/O ratios give rise to a greater abundance of carbon-rich molecules, which in turn makes the atmosphere more opaque and so hotter and less dense (see Fig. 3). Such conditions do not favour the formation of HCN/HNC. So a high C/O ratio can result in the destruction of HCN/HNC. These sensitivities to the C/O ratio at $T_{\rm eff} \sim 3000$ K make it difficult to fit spectra to the higher-temperature C stars, such as TX Psc (see Section 5.2.2).

As discussed in Section 3 we have obtained suitable spectra of the carbon-rich asymptotic giant branch (AGB) stars WZ Cas and TX Psc from the *ISO* archives. The inclusion of the new extensive HCN/HNC line list (Harris et al. 2002b) within our synthetic spectra allows the identification of HCN and HNC features within these stellar spectra. The new HCN/HNC are more complete, and in the

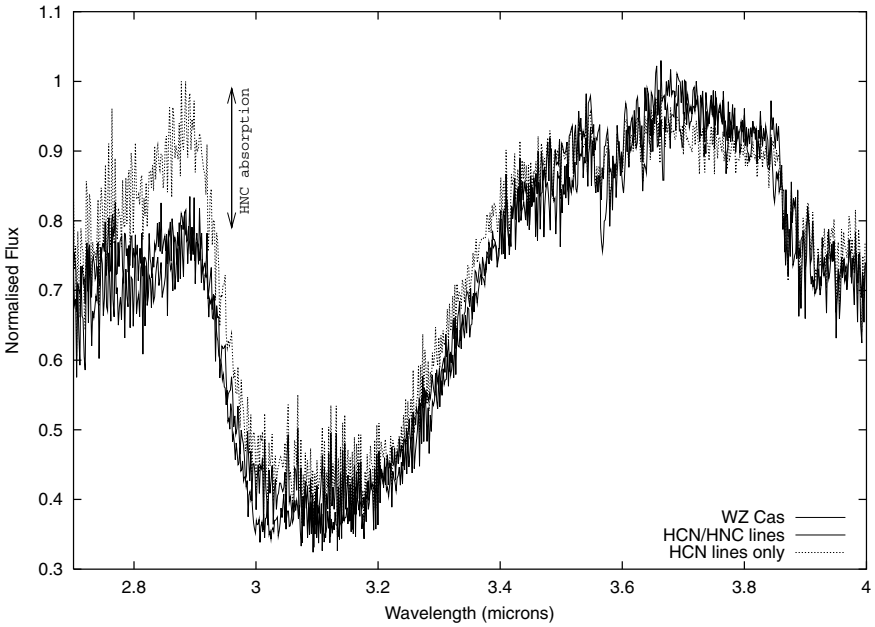

Figure 6. Synthetic spectra of carbon-rich atmospheres at $T_{\rm eff} = 2800$ K, log $(N_{\rm C}/N_{\rm O})$ of 0.003, with a $V_{\rm t} = 3.5$ km s^{-1} in the region 2.7–4.0 μm. The spectra were calculated with the full HCN/HNC line list of Harris et al. (2002b) and with only HCN lines selected. For comparison, the observed spectrum of WZ Cas is shown. The resolution of these spectra is 1.6 nm. This figure is available in colour in the online version of the journal on *Synergy*.

case of *ab initio* data more accurate, than the preceding HCN/HNC data and so allow the determination of new effective temperatures and C/O ratio for these stars.

5.2.1 WZ Cas

Fig. 6 shows the spectrum of WZ Cas together with the best-fitting synthetic spectrum calculated with HCN/HNC opacity and a synthetic spectrum calculated using only HCN opacity. Both of the synthetic spectra were computed for a model atmosphere of $T_{\rm eff} =$ 2800 K, a turbulent velocity of 3.5 km s^{-1} and a value of log $(N_{\rm C}/N_{\rm O})$ of 0.003. To permit easy identification of the broad absorption features within the spectra, both synthetic and observed spectra are shown at a resolution of 1.5 nm. Recent measurements and fits for the effective temperature and log $(N_{\rm C}/N_{\rm O})$ are shown in Table 1. There are large differences between the values of $T_{\rm eff}$. The estimate of $T_{\rm eff}$ from Dyck, van Belle & Benson (1996) is 350 K hotter than the estimate of $T_{\rm eff}$ from our models. However, if we use this $T_{\rm eff}$ in our models, HCN does not form in large enough quantities to form strong absorption features (see Fig. 4). There are large errors of 200 K on the value of $T_{\rm eff}$ quoted by Dyck et al. (1996). Our estimate of $T_{\rm eff}$ and log $(N_{\rm C}/N_{\rm O})$ for WZ Cas is closer to that of Lambert et al. (1986) and that of Aoki et al. (1998), which is a recalibration of the infrared flux method (IRFM) (Blackwell, Petford & Shallis 1980) determination by Ohnaka & Tsuji (1996).

In general the major features of the synthetic spectrum with both HCN and HNC opacity fit well the observed spectrum of WZ Cas. The absorption feature above 3.8 μm is attributable to a combination of the Q-branch absorption of the (0, 1, 1, 0) → (1, 0, 0, 0) band together with its hot bands and the $\Delta v = 2$ bands of CS. The general shape of this feature is well reproduced in both synthetic spectra. However, the positions of the individual Q branches in the synthetic spectra are slightly displaced from the same Q branches in the observed spectrum. This is a result of the errors on the line frequencies in the *ab initio* data of Harris et al. (2002b). There is slightly weaker absorption in this region in the synthetic spectrum with only HCN absorption than there is in the spectrum that uses the full HCN/HNC opacity. This is most likely a result of the effect of absorption by the HNC (0, 0, 0, 0) → (0, 1, 1, 1) band, centred on 4.03 μm, and its hot bands. From Fig. 1 it is expected that HNC will contribute to the overall HCN/HNC opacity in this region. Some of the changes in the synthetic spectra may also have been brought about by changes in the optical depth, pressure and temperature of the model atmosphere.

The absorption in the 3.6-μm region is attributable to the Q branches of the HCN (0, 0, 0, 0) → (0, 1, 1, 1) band. Again the general shape of this feature in both synthetic spectra is well

Table 1. Effective temperatures, C/O ratios and surface gravities for WZ Cas.

Work	$T_{\rm eff}$	log $(N_{\rm C}/N_{\rm O})$	log (g)	Notes
Lambert et al. (1986)	2850	0.0043		$T_{\rm eff}$ from colour indices, log $(N_{\rm C}/N_{\rm O})$ from models
Dyck et al. (1996)	3140±193			Interferometry
Aoki et al. (1998)	2900	0.0043	0.0	Recalibrated IRFM determination of Ohnaka & Tsuji (1996)
This work	2800	0.003	0.0	Model

reproduced, but the Q branches in the synthetic spectra are displaced from the observed spectra, a result of the error on the *ab initio* HCN/HNC data of Harris et al. (2002b). Shortwards of 3.55 μm the spectrum that contains both HCN and HNC absorption agrees well with the observed spectra. The spectrum that does not contain HNC data appears to be missing absorption, especially in the 2.9-μm region. The broad absorption feature from 2.95 to 3.4 μm is widely attributed to the H–C stretching fundamental of HCN, centred on 3.02 μm, and its hot bands. This region has been well documented in the past (for example Aoki et al. 1998). There should also be a little absorption from the C_2H_2 symmetric and antisymmetric H–C stretching modes. However, the difference between the intensity of this feature in the synthetic spectra with and without HNC suggests that much absorption in this region is a result of HNC. The strongest HNC mode in this region is the (0, 1, 1, 0) → (1, 0, 0, 0) band, centred on 3.125 μm, and its hot bands. The effect of this band on the combined HCN/HNC opacity can be seen in Fig. 1.

The biggest difference between the synthetic spectra with HCN/HNC lines and with only HCN lines lies in the 2.85-μm region. The dominant absorption in this region of the synthetic spectrum with only HCN opacity is caused by CO absorption from the $\Delta v = 2$ band. However, in the synthetic spectrum that includes the full HCN/HNC opacity there is additional absorption. This is the HNC (0, 0, 0, 0) → (1, 0, 0, 0) fundamental and hot bands, centred on 2.73 μm. From the *ab initio* absorption spectrum of HCN/HNC (Fig. 1) it would be expected that if HCN and HNC are in thermodynamic equilibrium there should be significant HNC absorption in this region. In the 2.85-μm region the differences between the observed and synthetic spectra are also at their greatest. The synthetic spectrum that includes the full HCN/HNC line list fits both the shape and flux of the spectrum of WZ Cas considerably better than does the synthetic spectrum that contains only HCN absorption. Thus it is here that we identify the effect of HNC absorption in the spectrum of a carbon star for the first time.

The synthetic spectra of Aoki et al. (1998) were calculated using available laboratory HCN data. Aoki et al. (1998) were not able to account fully for the HCN absorption between 3.8 and 4.2 μm, using only these laboratory data. To gain a closer agreement with observed spectra Aoki et al. (1998) had to estimate opacity empirically from $\Delta v_1 = 2$, $\Delta v_2 = -1$ hot bands with $v_2 > 5$. Our synthetic spectra do not suffer from this data deficit and are on the whole in good agreement in this region. The minimum frequency of the synthetic spectra of Aoki et al. (1998) is 2.9 μm, so we are unable to comment upon the spectra at 2.8 μm where HNC is a strong absorber.

For the spectral ranges 3.55 to 3.63 μm and 3.83 to 3.97 μm we plot the observed spectrum of WZ Cas together with the best-fitting synthetic spectrum in Figs 7 and 8, respectively. To help the reader identify the bands of HCN responsible for the absorption features in the synthetic and hence observed spectra, we have plotted the *ab initio* HCN Q-branch lines at the bottom of these figures. The band centres of the *ab initio* data of Harris et al. (2002b) are identified by the lower marks and digits, and the experimentally determined band centres by the upper marks and digits. The indices of the band centres are given in Tables 2 and 3. To show the relatively broad absorption features the resolution of both the observed and synthetic spectra has been set to 0.75 nm. The typical spacing between Q-branch lines in triatomics is considerably smaller (about 0.1 nm) than the spacing between P- and R-branch lines (about 4 nm). Consequently, the intensity of the P and R branches is distributed over a large wavelength range. Hence the P and R branches are broader and weaker than the Q branches, which are characterized by narrow and strong absorption. The effects of Q branches in the spectra are thus often more apparent than the effects of P and R branches. This is seen in both Figs 7 and 8. The absorption features correspond to the places in which the Q-branch lines are densest. Usually this corresponds to the position of the band centres. In some cases the line positions of Q-branch lines will increase in wavelength with J, and at some point reverse and decrease in wavelength with J, in

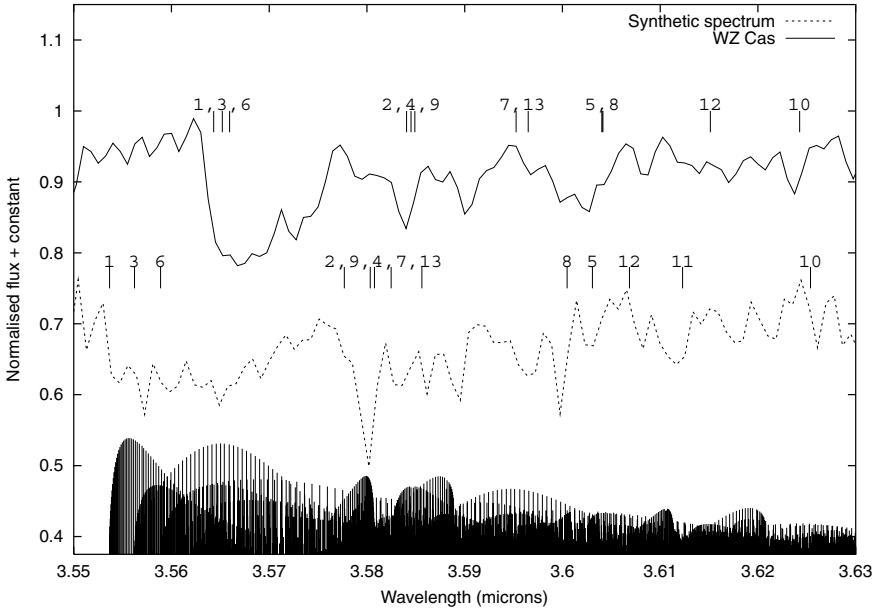

Figure 7. The observed spectrum of WZ Cas over the region of 3.55–3.61 μm, with a synthetic spectrum at $T = 2800$ K, log (N_C/N_O) of 0.003 and $V_t = 3.5$ km s^{-1}. A constant is subtracted from the flux of the synthetic spectrum to stagger it from the observed spectrum. The Q-branch lines in this spectral region in the *ab initio* data of Harris et al. (2002b) are plotted at the bottom of the figure with line length in proportion to intensity. The experimental band centres of the (0, 0, 0, 0) → (0, 1, 1, 1) band and its hot bands are indicated by the upper series of marks and digits. Likewise the lower series of marks and digits identify the band centres of the *ab initio* data of Harris et al. (2002b). The data for these bands, together with their indices, are tabulated in Table 2.

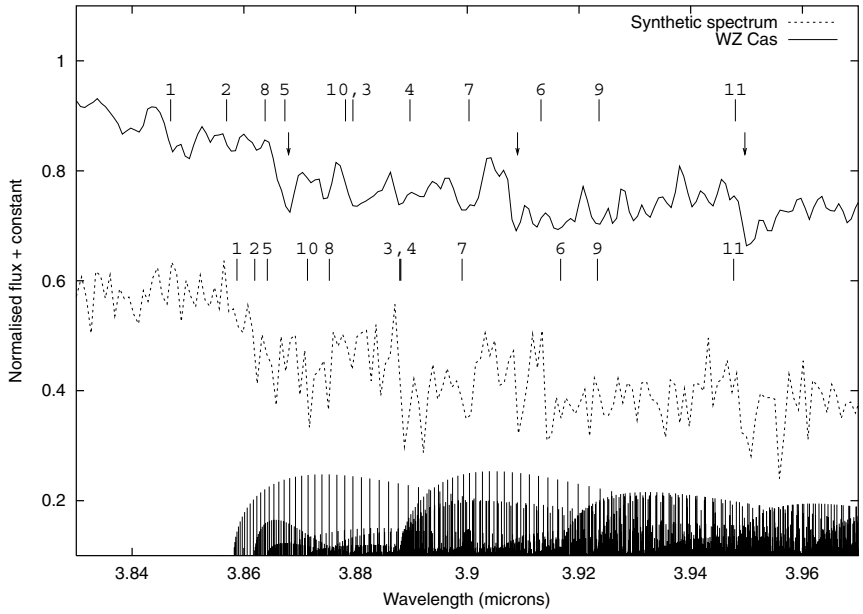

Figure 8. The observed spectrum of WZ Cas over the region of 3.8–4.0 μm, with a synthetic spectrum at $T = 2800$ K, log (N_C/N_O) of 0.003 and $V_t = 3.5$ km s^{-1}. A constant is subtracted from the flux of the synthetic spectrum to stagger it from the observed spectrum. The Q-branch lines in this spectral region in the *ab initio* data of Harris et al. (2002b) are plotted at the bottom of the figure with line length in proportion to line intensity. The experimental band centres of the (0, 1, 1, 0) → (1, 0, 0, 0) band and its hot bands are indicated by the upper series of marks and digits. Likewise the lower series of marks and digits identify the band centres of the *ab initio* data of Harris et al. (2002b). The downward pointing arrows indicate the position of CS bandheads. The data for the HCN bands, with their indices, are tabulated in Table 3.

Table 2. Laboratory and *ab initio* band centres for bands with $\Delta v_2 = 1$, $\Delta v_3 = 1$.

Index[a]	(v_1', v_2', l', v_3')	$(v_1'', v_2'', l'', v_3'')$	E_c' (cm^{-1})	E_c'' (cm^{-1})	Theory[b] λ_c (μm)	Expt[c] λ_c (μm)
1	(0,1,1,1)	(0,0,0,0)	2814.00	0.0	3.5537	3.5643
2	(0,2,0,1)	(0,1,1,0)	3510.99	715.89	3.5777	3.5841
3	(0,2,2,1)	(0,1,1,0)	3527.86	715.89	3.5562	3.5652
4	(0,3,1,1)	(0,2,0,0)	4207.62	1414.92	3.5808	3.5845
5	(0,3,1,1)	(0,2,2,0)	4207.62	1432.20	3.6031	3.6040
6	(0,3,3,1)	(0,2,2,0)	4242.07	1432.20	3.5589	3.5659
7	(0,1,1,2)	(0,0,0,1)	4891.95	2100.58	3.5825	3.5953
8	(0,4,0,1)	(0,3,1,0)	4891.76	2114.34	3.6005	3.6041
9	(0,4,2,1)	(0,3,1,0)	4907.37	2114.34	3.5803	3.5849
10	(0,4,2,1)	(0,3,3,0)	4907.37	2149.03	3.6254	3.6243
11	(0,4,4,1)	(0,3,3,0)	4957.36	2149.03	3.6123	–
12	(0,2,0,2)	(0,1,1,1)	5586.50	2814.00	3.6069	3.6151
13	(0,2,2,2)	(0,1,1,1)	5602.92	2814.00	3.5856	3.5965

[a]This is the index of the band used in Fig. 7.
[b]Calculated from the *ab initio* data of Harris et al. (2002b).
[c]From the laboratory measurements of Maki et al. (1996).

a similar fashion to a bandhead. For example, the feature at about 3.58 μm in the synthetic spectrum is attributable to a Q branch of the (0, 3, 1 f, 1) → (0, 4, 2 e, 1) band which displays such behaviour.

This comparison of the Q-branch line positions and intensities in Figs 7 and 8 with the synthetic spectra allows us to attribute some of the absorption features in the observed spectra to Q branches. In Fig. 7 the deep absorption at 3.567 μm in the spectrum of WZ Cas is attributable to the Q branches of the (0, 0, 0, 0) → (0, 1, 1, 1), (0, 1, 1, 0) → (0, 2, 2, 1), (0, 2, 2, 0) → (0, 3, 3, 1) bands and higher hot bands. The feature at 3.584 μm is attributable in the most part to the Q branches of the (0, 2, 0, 0) → (0, 3, 1, 1) and the (0, 3, 1, 0) → (0, 4, 2, 0) bands. The line spacing of the (0, 1, 1, 0) → (0, 2, 0, 1) is large, and consequently the intensity of the Q branch is spread over a larger wavelength range so is less detectable. Beyond 3.585 μm the increasing density of bands coupled with the errors on the *ab initio* data make it difficult to attribute absorption features to specific bands. The synthetic spectra of Aoki et al. (1998) reproduce the 3.56–3.63 μm band, but because of the limitations of their line list they were unable to fully explain the various features in this region. The match of the synthetic spectra to the observed spectrum would be much improved if better frequency data were used. It is possible to substitute experimentally determined HCN/HNC energy levels and hence line frequencies into the Harris et al. (2002b) line list. This would improve the line frequencies for all the lines corresponding to transitions between experimentally determined energy levels. However, this would require the manual assignment of the

Table 3. Laboratory and *ab initio* band centres for bands with $\Delta v_1 = 1$, $\Delta v_2 = -1$.

Index[a]	(v_1', v_2', l', v_3')	$(v_1'', v_2'', l'', v_3'')$	E_c' (cm^{-1})	E_c'' (cm^{-1})	Theory[b] λ_c (μm)	Expt[c] λ_c (μm)
1	(1,0,0,0)	(0,1,1,0)	3307.70	0.0	3.8588	3.8469
2	(1,1,1,0)	(0,2,0,0)	4004.28	1414.92	3.8620	3.8569
3	(1,1,1,0)	(0,2,2,0)	4004.28	1432.20	3.8879	3.8795
4	(1,2,0,0)	(0,3,1,0)	4686.28	2114.34	3.8881	3.8898
5	(1,2,2,0)	(0,3,1,0)	4702.19	2114.34	3.8642	3.8673
6	(1,2,2,0)	(0,3,3,0)	4702.19	2149.03	3.9167	3.9132
7	(1,3,1,0)	(0,4,0,0)	5366.17	2801.46	3.8991	3.9003
8	(1,0,0,1)	(0,1,1,1)	5394.43	2814.00	3.8753	3.8638
9	(1,3,1,0)	(0,4,2,0)	5366.17	2817.27	3.9233	3.9236
10	(1,3,3,0)	(0,4,2,0)	5400.32	2817.27	3.8714	3.8782
11	(1,3,3,0)	(0,4,4,0)	5400.32	2867.21	3.9477	3.9480

[a]This is the index of the band used in Fig. 8.
[b]Calculated from the *ab initio* data of Harris et al. (2002b).
[c]From the laboratory measurements of Maki et al. (1996).

'approximate' quantum numbers v_1, v_2, v_3 and l to many of the 125 000 energy levels included in the Harris et al. (2002b) line list. Barber et al. (2002) have already assigned about a quarter of the levels we needed to be able to insert experimentally determined energy levels.

The spectral region covered by Fig. 8 is slightly more complex, because there is significant absorption from both HCN and CS. The bandheads of the CS 0 → 1, 1 → 2 and 2 → 3 lie at 3.868, 3.909 and 3.9497 μm, respectively (Chandra et al. 1995). Three absorption features in the observed and synthetic spectrum of WZ Cas caused by these bandheads are clearly visible and have previously been commented upon by Aoki et al. (1998) in WZ Cas and TX Psc and also by Jørgensen et al. (2000) in TX Psc. As far as HCN absorption is concerned, the 3.85-μm feature in the spectrum of WZ Cas is attributable to the Q branch of the (0, 1, 1, 0) → (1, 0, 0, 0) band. The absorption at about 3.88 μm can be confidently associated with the Q branches of the (0, 2, 2, 0) → (1, 1, 1, 0) and (0, 4, 2, 0) → (1, 3, 3, 0) bands. There is also a strong case for the 3.9-μm absorption being caused by the unusually high density of Q-branch lines in the (0, 4, 0, 0) → (1, 3, 1, 0) band. It is also likely that the (0, 2, 0, 0) → (1, 1, 1, 0) band is responsible for the weak absorption at 3.857 μm in the spectrum of WZ Cas. The increasing density and decreasing strength of both HCN and CS lines coupled with the errors of the *ab initio* HCN data hinder further identifications longwards of 3.905 μm.

In this work we have assumed that the spectrum of $H^{13}CN$ is identical to that of $H^{12}CN$. In reality this is not the case: the vibrational band centres and rotational constants are slightly different. Maki et al. (2000) have measured band centres and rotational constants for $H^{13}CN$ in the laboratory. These measurements found the band centres of the $H^{13}CN$ fundamentals to be lower in wavenumber than those of $H^{12}CN$. The band centre of the fundamental of the C–N stretching mode differs by ∼1.6 per cent between the two isotopomers, the bending mode by ∼0.8 per cent and the H–C stretching mode by ∼0.5 per cent. If the abundance ratio of ^{13}C to ^{12}C is high in a star, then one would find that the absorption bands of HCN would have slightly different shapes. Furthermore there would be additional Q branches of $H^{13}CN$ in the spectra, which would be slightly displaced from those of $H^{12}CN$. When corrected for the change in centre of mass, the $H^{13}CN$ electric dipole moment is identical to that of $H^{12}CN$. Consequently the transition dipoles of the $H^{13}CN$ should be close to those of $H^{12}CN$. To gain a good approximation to the absorption of $H^{13}CN$, the experimental energy levels of $H^{13}CN$ could be substituted for the theoretical levels of $H^{12}CN$ in the Harris et al. (2002b) line list. This, however, must also wait until sufficient energy levels of the Harris et al. (2002b) line list are assigned.

5.2.2 TX Psc

Fig. 9 shows the *ISO* SWS spectrum of TX Psc, taken by Aoki et al. (1998), with our best-fitting synthetic spectra. One of the synthetic spectra is calculated with the full HNC/HCN opacity and the other is calculated with only HCN opacity. Both of the synthetic spectra are calculated with $T_{\rm eff} = 3050$ K, log (C/O) = 0.03, $V_t = 3.5$ km s^{-1} and log $(Z/Z_\odot) = -0.3$.

The $T_{\rm eff}$ and C/O ratio estimations for TX Psc of Aoki et al. (1998), Jørgensen et al. (2000) and this work are summarized in Table 4, together with interferometric estimates of $T_{\rm eff}$. All the values of $T_{\rm eff}$ deduced from the fitting of synthetic spectra agree to within 100 K, but the values obtained by interferometric means are up to 200 K cooler. Jørgensen et al. (2000) reported that their estimate of the $T_{\rm eff}$ of TX Psc changed from 3100 K to 3000 K between the two separate *ISO* observations, one taken by themselves and one taken by Aoki et al. (1998). However, such temperature variations are difficult to confirm, as the error in $T_{\rm eff}$ of our fit is around 100 K. The value of log $(N_C/N_O) = 0.015$ from our work is closer to the lower log $(N_C/N_O) = 0.010$ value of the two good fits of Jørgensen et al. (2000) than the higher values of 0.041–0.068 (Aoki et al. 1998; Jørgensen et al. 2000; Ohnaka, Tsuji & Aoki 2000). In our synthetic spectra the HCN absorption features are very weak for values of log (N_C/N_O) greater than 0.02 (see Fig. 5). So we believe the lower log (N_C/N_O) values for TX Psc are closer to the real values.

There are dramatic differences between the two synthetic spectra shown in Fig. 9. The broad 3.1-μm absorption feature in the synthetic spectrum with HCN and HNC opacity is much weaker in the synthetic spectrum calculated with only HCN opacity. At $T_{\rm eff} =$ 3000 K the model atmospheres are very sensitive; slight changes in temperature and log (N_C/N_O) can have a dramatic effect on the synthetic spectra (for example see Figs 4 and 5). As discussed in Section 5.1, a model without HNC opacity has a higher temperature and pressure at a given optical depth than a model with the full HCN/HNC opacity. Hence a reduction in opacity caused by neglecting HNC opacity can affect the structure of the atmosphere to the extent that HCN absorption is dramatically reduced. As in the case of WZ Cas both HCN and HNC are required to explain the observed spectra. Marked on Fig. 9 are the 0 → 1, 1 → 2 and 2 →

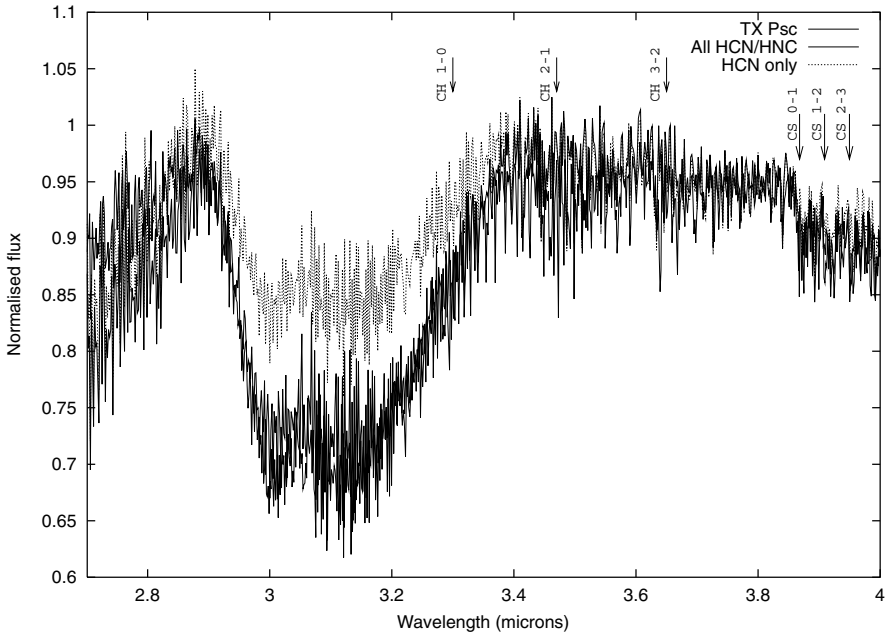

Figure 9. Synthetic spectra of carbon-rich atmospheres at $T_{\rm eff} = 3050$ K with $V_{\rm t} = 3.5$ km s^{-1} and log $(N_{\rm C}/N_{\rm O}) = 0.015$ in the region 2.7–4.0 μm. The spectra were calculated with the full HCN/HNC line list of Harris et al. (2002b) and with just HCN lines selected from the Harris et al. (2002b) line list (see text). For comparison, the observed spectrum of TX Psc is shown. We have also indicated with arrows the positions of CS and CH bandheads. The resolution of these spectra is 1.6 nm. This figure is available in colour in the online version of the journal on *Synergy*.

Table 4. Effective temperatures, log $(N_{\rm C}/N_{\rm O})$ and surface gravities for TX Psc.

Work	$T_{\rm eff}$	log $(N_{\rm C}/N_{\rm O})$	log (g)	Notes
Lambert et al. (1986)	3030	0.012		$T_{\rm eff}$ from colour index, log $(N_{\rm C}/N_{\rm O})$ from models
Quirrenbach et al. (1994)	2805±126			Interferometry
Dyck et al. (1996)	2921±60			Interferometry
Aoki et al. (1998)	3100	0.041	0.0	Recalibrated IRFM determination of Ohnaka & Tsuji (1996)
Jørgensen et al. (2000)	3100	0.01	−0.5	Model
	3100	0.041	0.0	Model
	3000	0.01	−0.5	Model
	3000	0.041	0.0	Model
Ohnaka et al. (2000)	3000	0.03	0.0	Model
	3100	0.068	0.0	Model
	3000	0.041	−0.5	Model
This work	3050	0.015	0.0	Model

3 CS and CH bandheads, which were identified previously by Aoki et al. (1998).

Although the synthetic spectra calculated with HCN/HNC opacity fit the observed spectrum well between 2.9 and 4.0 μm, there is a slight underprediction of the strength of the absorption between 3.0 and 3.2 μm. Between 2.7 and 2.9 μm the flux from the synthetic spectrum dips to below the spectrum of TX Psc. The absorption across this region is effected by the tail of the CO $\Delta v = 2$ bands. The effect of this CO band is evident in the synthetic spectra shown in Fig. 5. This would imply that there is too much CO within our model atmosphere. We have looked at other potential ways of reducing the abundance of CO, including changing the surface gravity and increasing and decreasing the value of log $(N_{\rm N}/N_{\rm O})$ above and below the solar value. It is clear that both these parameters do affect the HCN absorption features in the final synthetic spectrum, but we have not found a better fit. The elemental abundances within carbon stars are not well known, so log $(N_{\rm C}/N_{\rm H})$, log $(N_{\rm N}/N_{\rm H})$, log $(N_{\rm O}/N_{\rm H})$ or indeed log $(N_{\rm He}/N_{\rm H})$ are not well constrained by observational data. With so many free parameters it is possible there are other good fits that we have not found.

6 CONCLUSION

We have calculated new model atmospheres and synthetic spectra for carbon stars, using the recent *ab initio* HCN/HNC line list of Harris et al. (2002b). However, selectively removing HNC lines from the HCN/HNC line list and recalculating our models, we have shown that HNC opacity can have a small but significant effect upon the structure of carbon-star atmospheres. The general shape of the pressure–temperature curves of our model atmospheres that exclude

HNC are consistent with those of Aoki et al. (1998) and Jørgensen et al. (2000). However, our models with both HCN and HNC will differ from those of Aoki et al. (1998) and Jørgensen et al. (2000), especially at low effective temperatures $T_{\rm eff} < 2900$ K and low $\log(N_{\rm C}/N_{\rm O}) < 0.01$.

We have obtained good fits of our synthetic spectra to the observed spectra of WZ Cas and TX Psc. These fits have provided a new independent estimate of the C/O ratio and $T_{\rm eff}$ of these stars. In general our estimate of the $T_{\rm eff}$ and C/O ratio for WZ Cas and TX Psc are in agreement with earlier works. For WZ Cas our $T_{\rm eff}$ and C/O ratio are both slightly lower than earlier estimates, which is consistent with an increase in overall opacity within the model due to the inclusion of HNC. For TX Psc our C/O ratio is towards the lower end of the earlier estimates of the C/O ratio. Our models using values of $\log(N_{\rm C}/N_{\rm O})$ greater than 0.02 favoured by earlier works cannot reproduce the observed spectra of TX Psc. However, by changing the many free parameters, such as $\log g$, $\log(N_{\rm C}/N_{\rm O})$, $\log(N_{\rm N}/N_{\rm O})$ and $T_{\rm eff}$, it may be possible to obtain other good fits, for example Jørgensen et al. (2000) obtained two good fits with different values of $\log(N_{\rm C}/N_{\rm O})$, $T_{\rm eff}$ and $\log g$.

By comparing our synthetic spectra calculated with and without HNC opacity, we have identified the contribution of HNC at 2.9 μm to the spectrum of WZ Cas for the first time. Absorption resulting from the Q-branch lines of the HCN $\Delta v_2 = 1$, $\Delta v_3 = 1$ and $\Delta v_1 = 1$, $\Delta v_2 = -1$ bands has been identified in the spectrum of WZ Cas. It has been shown that, to model the atmospheres of C stars correctly, opacity arising from HNC must be accounted for.

It may be possible to correct for systematic errors in line frequencies of the line list of Harris et al. (2002b) by substituting experimentally determined energy levels for their *ab initio* counterparts. This would give very accurate line frequencies for the lines corresponding to transitions between the experimentally determined energy levels. Similarly, by substituting experimentally determined $H^{13}CN$ energy levels for their *ab initio* $H^{12}CN$ counterparts, it should be possible to account better for the spectrum of $H^{13}CN$. This, however, must await the assignment of approximate quantum numbers to the energy levels of the line list of Harris et al. (2002b).

ACKNOWLEDGMENTS

Our referee Wako Aoki is thanked for helpful comments, which have served to improve this paper. We thank the UK Particle Physics and Astronomy Research Council (PPARC) for post-doctoral funding for GJH. PPARC and the Royal Society are thanked for travel grants. The work of YP is partially supported by a research grant from the American Astronomical Society. The manipulation and analysis of the HCN/HNC line list was carried out on the Miracle 24-processor Origin 2000 supercomputer at the HiPerSPACE computing centre, UCL, which is part funded by PPARC.

REFERENCES

Anders E., Grevesse N., 1989, Geochim. Cosmochim. Acta, 53, 197
Aoki W., Tsuji T., Ohnaka K., 1998, A&A, 340, 222
Aoki W., Tsuji T., Ohnaka K., 1999, A&A, 350, 945
Barber R. J., Harris G. J., Tennyson J., 2002, J. Chem. Phys., 117, 11239
Blackwell D. E., Petford A. D., Shallis M. J., 1980, A&A, 82, 249
Chandra S., Kegel W. H., Le Roy R. J., Hertenstein T., 1995, A&AS, 114, 175
Doyle R. O., 1968, ApJ, 153, 987
Dyck H. M., van Belle G. T., Benson J. A., 1996, AJ, 112, 294
Eriksson K., Gustafsson B., Jørgensen U. G., Nordlund Å., 1984, A&A, 132, 37
Goorvitch D., 1994, ApJSS, 95, 535
Harris G. J., Polyansky O. L., Tennyson J., 2002a, Spectrochim. Acta A, 58, 673
Harris G. J., Polyansky O. L., Tennyson J., 2002b, ApJ, 578, 657
Jørgensen U. G., Almlöf J., Gustafsson B., Larsson M., Siegbahn P., 1985, J. Chem. Phys., 83, 3034
Jørgensen U. G., Hron J., Loidl R., 2000, A&A, 356, 253
Kupka F., Piskunov N., Ryabchikova T. A., Stempels H. C., Weiss W. W., 1999, A&AS, 138, 119
Kurucz R. L., 1993, (http://cfa-www.harvard.edu/amdata/ampdata/kurucz18/)
Kurucz R. L., 1996, in Adelman S., Kupka F., Weiss W. W., eds, ASP Conf. Ser. Vol. 108, Model Atmospheres and Stellar Spectra. Astron. Soc. Pac., San Francisco, p. 160
Lambert D. L., Gustafsson B., Eriksson K., Hinkle K. H., 1986, ApJSS, 62, 373
Loidl R., Höfner S., Jørgensen U. G., Aringer B., 1999, A&A, 342, 531
Loidl R., Lançon A., Jørgensen U. G., 2001, A&A, 371, 1065
Maki A., Quapp W., Klee S., 1995, J. Mol. Spectrosc., 171, 420
Maki A., Quapp W., Klee S., Mellau Ch. G., Albert S., 1996, J. Mol. Spectrosc., 180, 323
Maki A., Mellau Ch. G., Klee S., Winnewisser M., Quapp W., 2000, J. Mol. Spectrosc., 202, 67
Myerscough V. P., McDowell M. R. C., 1966, MNRAS, 132, 457
Nersisian S. E., Shavrina A. V., Yakemchuk A., 1989, Astrofisika, 20, 249
Ohnaka K., Tsuji T., 1996, A&A, 310, 933
Ohnaka K., Tsuji T., Aoki W., 2000, A&A, 353, 528
Pavlenko Ya. V., 1997, Astron. Astrophys Sci., 253, 43
Pavlenko Ya. V., 2000, Astron. Rep., 44, 219
Pavlenko Ya. V., 2002a, in Piskunov N., ed., Proc. IAU 210, Modelling of stellar atmospheres. Astron. Soc. Pac., San Francisco, in press (astro-ph 0209022)
Pavlenko Ya. V., 2002b, Astron. Rep., 46, 567
Pavlenko Ya. V., 2003, Astron. Rep., 47, 59
Pavlenko Ya. V., Zhukovska S., 2003, Kinematika i Fisika Nebesnych tel., 19, 28
Quirrenbach A., Mozurkewich D., Hummel C. A., Buscher D. F., Armstrong J. T., 1994, A&A, 285, 541
Salama A. et al., 1997, in Heras A. M., Leech K., Trams N. R., Perry M., eds, ESA ISO workshop on Analytical Spectroscopy. ESA SP-419, Noordwijk, p. 17
Seaton M. J., Zeipen C. J., Tully J. A., 1992, Rev. Mex. Astron. Astrophys., 23, 107
Sneden C., Johnson H. R., Krupp B. M., 1976, ApJ, 204, 218
Tsuji T., 1973, A&A, 23, 411
Unsold A., 1955, Physik der Sternatmospharen, 2nd edn. Springer-Verlag, Berlin
van Mourik T., Harris G. J., Polyansky O. L., Tennyson J., Császár A. G., Knowles P. J., 2001, J. Chem. Phys., 115, 3706

This paper has been typeset from a TEX/LATEX file prepared by the author.